Arch. Metall. Mater., Vol. 61 (2016), No 3, p. 1715–1722

DOI: 10.1515/amm-2016-0252

F. ZHAO*, C.L. ZHANG*, Y.Z. LIU*,#

FERRITE DECARBURIZATION OF HIGH SILICON SPRING STEEL IN THREE TEMPERATURE RANGES

Surface decarburization of high silicon spring steel in ambient air was studied. The experimental results confirmed the decarburized mechanism under A_{C1} temperature, in the temperature range of A_{C1}-A_{C3} and A_{C3}-G. Under A_{C1} temperature, pearlite spheroidization and surface decarburization are carried out simultaneously and pearlite spheroidization is reinforced. Considering the oxidation loss depth, the "true ferrite decarburized depth" at 850 °C (A_{C3}-G) is still smaller than that at 760°C (A_{C1}-A_{C3}). That is because an "incubation period" must pass away before ferrite decarburization occurs in the temperature range of A_{C3}-G, and the ferrite decarburized rate is limited to being equal to the partial decarburized rate.

Keywords: Surface decarburization; Steel; Oxidation; Carbon diffusion

1. Introduction

Surface decarburization is one of the common scientific problems in the quality control of medium or high carbon steel [1-4]. The high silicon spring steel can suffer from severe decarburization, which greatly influences the material properties, such as strength, hardness and fatigue resistance [5-7]. The fatigue limit can compromise dramatically if the ferrite decarburization forms [8]. The ferrite decarburization is not allowed in some national standards on spring steel, such as ASTM A232, JIS G3565 and GB/T 1222. On the other hand, according to recent investigation, the ferrite decarburization can also be used to make compositionally graded materials [9,10]. It's very important to make the mechanism of ferrite decarburization clear.

It was reported that ferrite decarburization can be produced in the temperature range of A_{C1}-G through the γ→α phase transformation [1,11]. The ferrite decarburization forming at A_{C1}-A_{C3} temperature was reported to be deeper than that forming at A_{C3}-G temperature when high silicon spring steel was heated for 1.5h [12]. Usually, the explanation about this phenomenon is that the oxidation loss rate increases faster than the decarburized rate with the rise of temperature, but this may also be related to the different decarburized mechanism between the two temperature ranges. Ferrite decarburization can also be produced under the A_{C1} temperature through the cementite dissolution [13], but the decarburized type and mechanism haven't been studied comprehensively.

There are a lot of reports about experimental study of the ferrite decarburized behavior. However, differences among decarburization in the three temperature ranges mentioned above have not been studied clearly. What's more, the influence of oxidation loss on the decarburized rate is not clear. Our study focused on the decarburized mechanism and the reason of different decarburized rate in three temperature ranges. It is believed that the data obtained could give a further insight into ferrite decarburization.

2. Experimental

The steel selected for this investigation was obtained from a commercial hot-rolled wire of 12 mm in diameter by a high-speed wire mill and has the chemical composition (wt%) of 0.60 C, 0.75 Mn, 1.69 Si, 0.14 Cr, 0.011 P and 0.008 S. The A_{C1} and A_{C3} temperature of the steel are 752 °C and 775 °C, respectively.

To avoid the effect of surface decarburization as rolled condition, samples with the size of 2×6×10 mm were cut at the center of the wires. Following the heat treatment program shown in TABLE 1, the specimens were heated in ambient air by SX-G07102 box furnace or Gleeble-1500. The heating temperature was controlled within ±2 °C by standardized thermocouple.

All the decarburized specimens were polished and etched with 4vol% nital for microstructural observation. The ferrite decarburized depth was measured ten times for each specimen by micrographic method. The partial decarburized depth was measured by hardness method. The oxidization loss depth was measured by comparing the specimens' optical micrographs at the same location before heating and after heating, which is shown in Fig. 1.

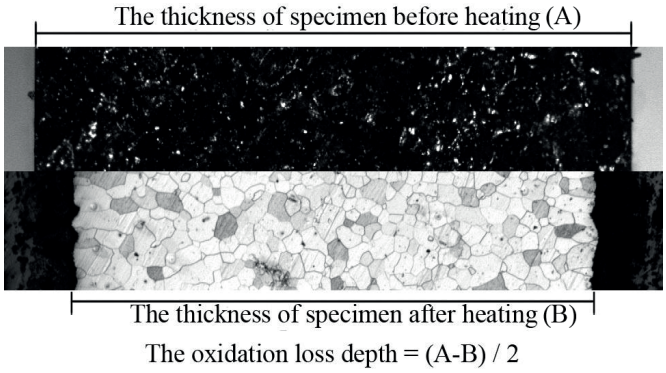

Fig. 1. The measure of oxidation loss depth

* SCHOOL OF MATE RIALS SCIENCE AND ENGINEERING, UNIVERSITY OF SCIENCE AND TECHNOLOGY BEIJING, BEIJING

Corresponding author: lyzh@ustb.edu.cn

3. Results and discussion

3.1. The surface decarburized mechanisms in different temperature ranges

3.1.1. The surface decarburized mechanism under A_{C1} temperature

After heating at 730 °C for 4 h then cooling by air, the surface decarburization is shown in Fig. 2. The spheroidizing degree of pearlite is higher at the area closer to ferrite decarburized layer.

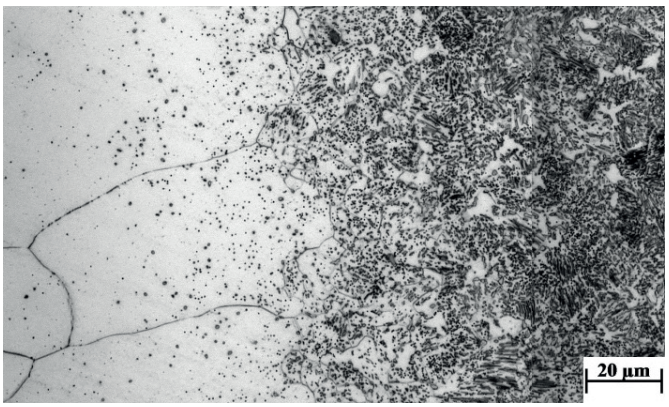

Fig. 2. Surface decarburization after heating at 730 °C for 4 h then cooling by air

The spheroidization of pearlite is coming along with the cementite dissolution. As shown in Fig. 3, with the cementite dissolution, a carbon concentration gradient forms near the cementite. The surface decarburization could enhance the carbon concentration gradient through diffusing the carbon away, so the carbon diffusion from cementite to ferrite is promoted. On the other hand, the decarburization can be carried out through the cementite dissolution. Consequently, under the A_{C1} temperature, pearlite spheroidization and surface decarburization are carried out simultaneously and pearlite spheroidization is reinforced.

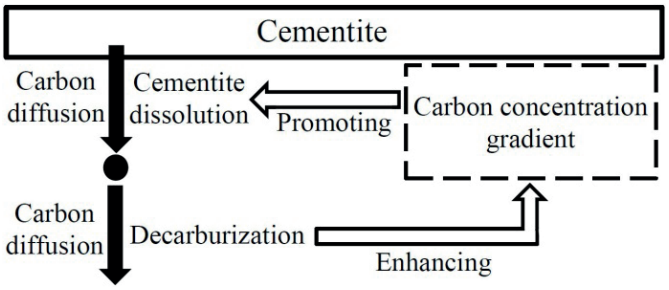

Fig. 3. The mutual reinforcement between pearlite spheroidization and decarburization

The hardness gradient curve of surface decarburization at 730 °C for 4 h is given in Fig. 4. The gradual increasing hardness indicates that ferrite decarburization and partial decarburization are both produced under A_{C1} temperature. The partial decarburization is made up of cementite particle + ferrite matrix and degenerated pearlite.

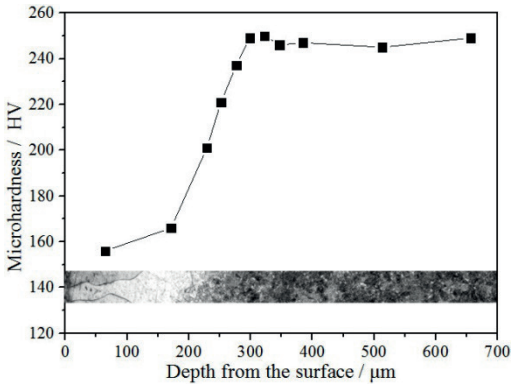

Fig. 4. Hardness gradient curve of surface decarburization at 730 °C for 4 h

3.1.2. The surface decarburized mechanism in the temperature range of A_{C1}-A_{C3}

After heating at 760 °C for 5 min then quenching by water and heating at 760 °C for 4 h then cooling by air, respectively, the surface decarburization is shown in Fig. 5.

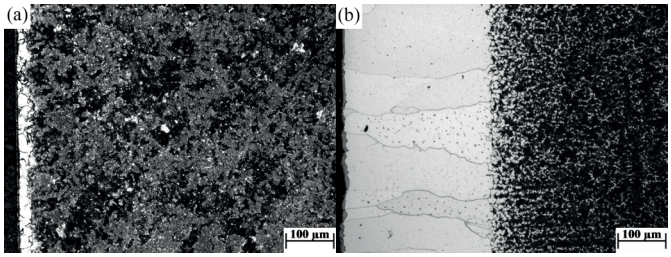

Fig. 5. Surface decarburization after heating at 760 °C: (a) 5 min, water quenching; (b) 4 h, air cooling

As shown in Fig. 5, both ferrite and partial decarburized layers formed in the temperature range of A_{C1}-A_{C3}, and ferrite decarburization started forming when soaking time was as short as 5 min. The schematic drawing of ferrite decarburization in the temperature range of A_{C1}-A_{C3} is shown in Fig. 6. Decarburization proceeded in the α+γ phase field all the time. According to Gibbs phase rule, the number of freedom degrees is zero in the two phase field at temperature and pressure constant, which suggests that the carbon concentration can't change freely, so the ferrite decarburization was produced

TABLE 1

Heat treatment program

Heating temperature / °C		Soaking time	Heating Equipment	Cooling method
< A_{C1}	730	1 h, 2 h, 4 h, 8 h	Furnace	Air cooling & Water quenching
A_{C1}-A_{C3}	760	1 h, 2 h, 4 h, 8 h		
A_{C3}-G	850	1 h, 2 h, 4 h, 8 h		
		5 min, 10 min, 15 min	Gleeble-1500	

through γ→α phase transformation. Ferrite formed around the austenite grain boundary nearby ferrite decarburization layer, so a thin partial decarburized layer formed, too.

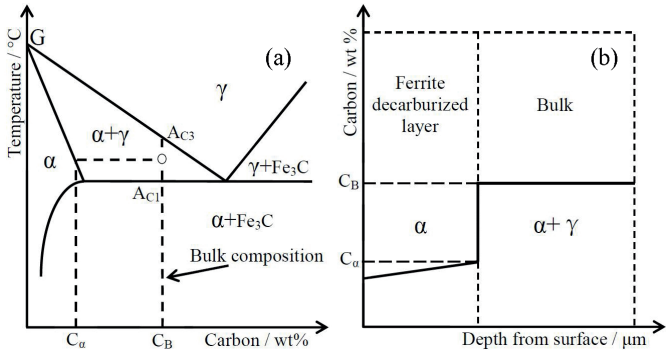

Fig. 6. schematic drawing of decarburization in the temperature range of A_{C1}-A_{C3}: (a) schematic phase diagram in Fe–C binary system; (b) schematic carbon concentration profile

3.1.3. The surface decarburized mechanism in the temperature range of A_{C3}-G

After heating at 850 °C for 5 min then quenching by water and heating at 850 °C for 4 h then cooling by air, respectively, the surface decarburization is shown in Fig. 7.

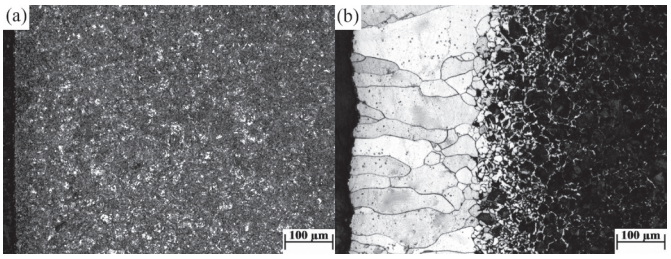

Fig. 7. Surface decarburization after heating at 850 °C: (a) 5 min, water quenching; (b) 4 h, air cooling

As shown in Fig. 7, the ferrite decarburization didn't occur after soaking for 5 min, and the decarburization was made up of the outer ferrite decarburization zone and the inner partial decarburization zone after soaking for 4 h. The schematic drawing of ferrite decarburization in the temperature range of A_{C3}-G is shown in Fig. 8. In the temperature range of A_{C3}-G, the carbon concentration is C_B in the γ single-phase region at the beginning. According to Gibbs phase rule, the number of freedom degrees is one in the single phase field at temperature and pressure constant, which suggests that the carbon concentration can change freely, so a partial decarburized layer which is in γ single-phase region formed with the carbon concentration continuously changes in C_B-$C_γ$. The ferrite decarburization formed when the carbon concentration went into the α+γ phase field with the decarburization proceeding. Unlike the decarburization in the temperature range of A_{C1}-A_{C3}, an "incubation period" must pass away before ferrite decarburization starts forming in the temperature range of A_{C3}-G.

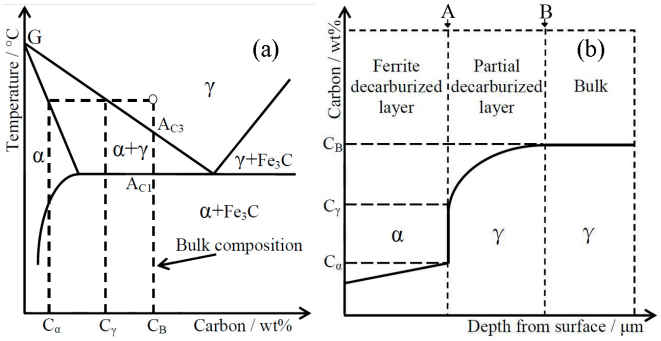

Fig. 8. schematic drawing of decarburization in the temperature range of A_{C3}-G: (a) schematic phase diagram in Fe–C binary system; (b) schematic carbon concentration profile

3.2. The mathematical model of ferrite decarburization at different temperature

The surface decarburized depth after heating at 730 °C, 760 °C and 850 °C for different soaking time is shown in TABLE 2.

3.2.1. The mathematical model of ferrite decarburization at 730 °C (< A_{C1})

Under A_{C1} temperature, the ferrite decarburization processes through the dissolution of cementite and the carbon diffusion in ferrite. According to Fick's first law, the increase of ferrite decarburized depth follows a parabolic law with the increase of the soaking time, which is shown in the Eq. (1):

$$h_{FI} = \mathrm{F_1}\sqrt{\mathrm{D}_\alpha t} \tag{1}$$

where h_{FI} is the increase of ferrite decarburized depth / m, t is the soaking time / s, F_1 is a constant coefficient when heating temperature is constant, $D_α$ is the diffusion coefficient of carbon in ferrite / ($m^2 \cdot s^{-1}$). Meanwhile, according to Fick's first law, the decrease of ferrite decarburized depth caused by oxidation can be got from the Eq. (2):

$$h_{OI} = \mathrm{O_1}\sqrt{t} \tag{2}$$

where h_{OI} is the decrease of ferrite decarburized depth / m, O_1 is a constant coefficient / ($m \cdot s^{-1/2}$) when heating temperature

TABLE 2

Surface decarburized depth after heating at different temperature for different time

Soaking time	5 min	10 min	15 min	1 h	2 h	4 h	8 h
< A_{C1}: 730 °C, ferrite decarburized depth / μm	--	--	--	80	131	196	285
A_{C1}-A_{C3}: 760 °C, ferrite decarburized depth / μm	--	--	--	148	226	308	452
A_{C3}-G: 850 °C, ferrite decarburized depth / μm	0	0	32	106	182	268	403
A_{C3}-G: 850 °C, partial decarburized depth / μm	--	--	--	150	155	161	156

is constant. Above all, under A_{C1} temperature, the ferrite decarburized depth follows a parabolic law with the increase of the soaking time, which is shown in the Eq. (3):

$$h_1 = h_{F1} - h_{O1} = F_1\sqrt{D_\alpha t} - O_1\sqrt{t} = K_1\sqrt{t} \quad (3)$$

where h_1 is the ferrite decarburized depth / m, K_1 is a constant coefficient / ($m \cdot s^{-1/2}$) when heating temperature is constant. K_1 can be found by the method of least squares curve fitting, as given in Eq. (4):

$$K_1 = \sqrt{\frac{\sum_{i=1}^{4} L_i^4}{\sum_{i=1}^{4}(t_i \bullet L_i^2)}} \quad (4)$$

where Li is experimentally measured decarburized depth / m, t_i is the soaking time / s. According to the ferrite decarburized depth and the soaking time in TABLE 2, one coefficient K_1 can be estimated. Then, functional relation between the ferrite decarburized depth and the soaking time at 730 °C can be established as Eq. (5), which is shown in Fig. 9. The error bars show the standard deviation, which is caused by repeated measurement.

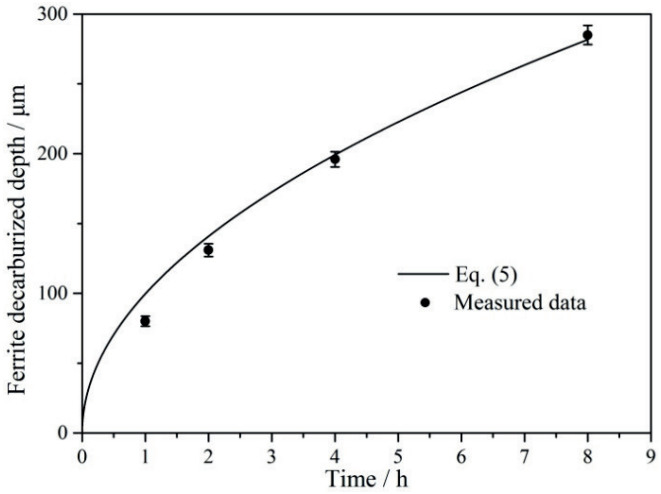

Fig. 9. Relationship between ferrite decarburized depth and soaking time at 730 °C

$$h_1(\mathrm{m}) = 1.66 \times 10^{-6}\sqrt{t(\mathrm{s})} \quad (5)$$

3.2.2. The mathematical model of ferrite decarburization at 760 °C (A_{C1}-A_{C3})

In the temperature range of A_{C1}-A_{C3}, the ferrite decarburization processes through γ→α phase transformation and carbon diffusion in ferrite. It's well known that the increase of ferrite depth can be obtained from the Eq. (6) [14]:

$$h_{F2} = \sqrt{\frac{6C_\alpha}{3C_B - 2C_\alpha}} \times \sqrt{D_\alpha t} = F_2\sqrt{D_\alpha t} \quad (6)$$

where h_{F2} is the increase of ferrite decarburized depth / m, t is the soaking time / s, D_α is the diffusion coefficient of carbon in ferrite / ($m^2 \cdot s^{-1}$), C_α and C_B are shown in Fig. 6 and both constant when heating temperature is constant, so F_2 is a constant coefficient. Meanwhile, according to Fick's first law, the decrease of ferrite decarburized depth caused by oxidation can be got from the Eq. (7):

$$h_{O2} = O_2\sqrt{t} \quad (7)$$

where h_{O2} is the decrease of ferrite decarburized depth / m, O_2 is a constant coefficient / ($m \cdot s^{-1/2}$) when heating temperature is constant. Above all, in the temperature range of A_{C1}-A_{C3}, the ferrite decarburized depth follows a parabolic law with the increase of the soaking time, which is shown in the Eq. (8):

$$h_2 = h_{F2} - h_{O2} = F_2\sqrt{D_\alpha t} - O_2\sqrt{t} = K_2\sqrt{t} \quad (8)$$

where h_2 is the ferrite decarburized depth / m, K_2 is a constant coefficient / ($m \cdot s^{-1/2}$) when heating temperature is constant. K_2 can be found by the method of least squares curve fitting. Then, functional relation between the ferrite decarburized depth and the soaking time at 760 °C can be established as Eq. (9), which is shown in Fig. 10. The error bars show the 1standard deviation, which is caused by repeated measurement.

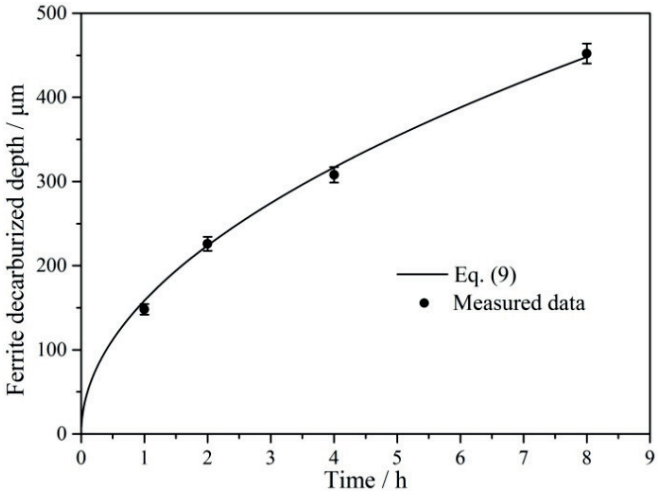

Fig. 10. Relationship between ferrite decarburized depth and soaking time at 760 °C

$$h_2(\mathrm{m}) = 2.64 \times 10^{-6}\sqrt{t(\mathrm{s})} \quad (9)$$

3.2.3. The mathematical model of ferrite decarburization at 850 °C (A_{C3}-G)

Both ferrite and partial decarburization formed in the temperature range of A_{C3}-G. As shown in Fig. 8, ferrite decarburization won't occur until matrix carbon concentration C_B reduces to C_γ, which means an "incubation period" has passed away. As shown in Fig. 11 and TABLE 2, the ferrite decarburization didn't occur when soaking time was 10 min, but it occurred when soaking time was 15

min, so the "incubation period" was confirmed to be about 12.5 min.

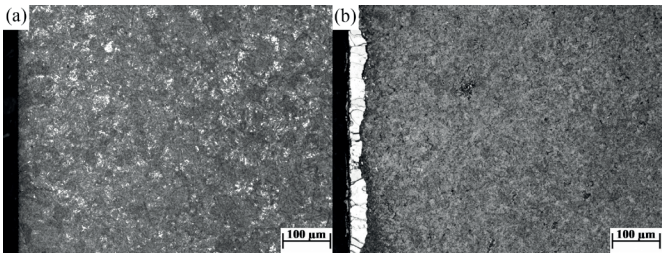

Fig. 11. Surface decarburization after heating at 850 °C then water quenching: (a) 10 min; (b) 15 min

Put the start time of ferrite decarburization to be the zero point of time axis, so a new set of data is gotten, which is shown in TABLE 3.

Now we can see a very interesting result. With the soaking time increasing, the ferrite decarburized depth increases continuously, but the partial decarburized depth stays constant at 850 °C. As shown in Fig. 8(b), the partial decarburized depth is controlled by diffusion of carbon in austenite matrix and γ→α phase transformation at the interface between ferrite and partial decarburization. If the partial decarburized depth is constant, the movement speed of interface A and B must be equal. Because only the carbon concentration at the interface A decrease to C_γ that ferrite decarburization can go on, we can know that the ferrite decarburized rate is limited to being equal to the partial decarburized rate, which is caused by slower carbon diffusion in austenite than that in ferrite.

According to Fick's first law, the increase of partial decarburized depth follows a parabolic law with the increase of the soaking time, so the ferrite decarburized depth also follows a parabolic law with the increase of the soaking time, which is shown in the Eq. (10):

$$h_3 = K_3\sqrt{t} \tag{10}$$

K_3 can be gotten with the same method in 3.2.1. Considering the "incubation period", functional relation between the ferrite decarburized depth and the soaking time at 850 °C can be established as Eq. (11), which is shown in Fig. 12. The error bars show the standard deviation, which is caused by repeated measurement.

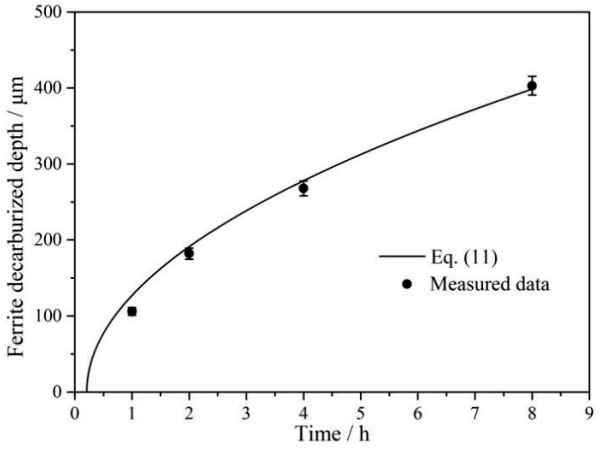

Fig. 12. Relationship between ferrite decarburized depth and soaking time at 850 °C

$$h_3(\mathrm{m}) = 2.38 \times 10^{-6}\sqrt{t(\mathrm{s}) - 750} \tag{11}$$

As shown in Fig. 13, the ferrite decarburized depth - soaking time curves at 730 °C, 760 °C and 850 °C can be put in a same coordinate axis. The ferrite decarburized rate at 760 °C is the biggest, and that at 850 °C takes the second place. Because the chemical bond of Fe_3C is more potent on fixing carbon than austenite, the dissolution of cementite is slow and the decarburized rate at 730 °C is far lower than that in the other two temperature ranges. When the specimen is heated for a short time, the "incubation period" for ferrite decarburization occurring at 850 °C has a signally effect on the ferrite decarburized depth.

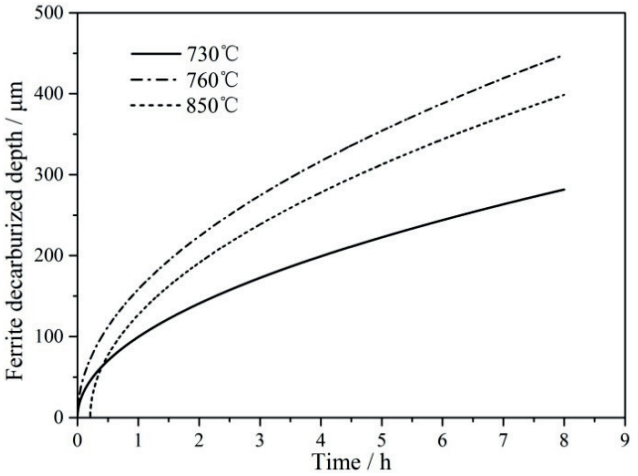

Fig. 13. The ferrite decarburization depth - soaking time curves at 730 °C, 760 °C and 850 °C

TABLE 3

The new set of data of surface decarburized depth after heating at 850 °C

Soaking time / s	0	2850	6450	13650	28050
Ferrite decarburized depth / μm	0	106	182	268	403
Partial decarburized depth / μm	--	153	162	160	156

3.3. Relationship between ferrite decarburization and oxidation loss

As shown in TABLE 4, in order to clear the influence of oxidation loss on ferrite decarburization, the oxidation loss depth after heating at 760 °C and 850 °C for different soaking time is measured.

As shown in TABLE 5, the start time of ferrite decarburization at 850 °C is also set to be the zero point of time axis, so a new set of data is gotten. The oxidation at 850 °C is faster than that at 760 °C because of the higher heating temperature.

As shown in TABLE 6, the oxidation loss depth is added up to ferrite decarburized depth to eliminate the influence of oxidation loss. The new depth is named "true ferrite decarburized depth".

Functional relation between the "true ferrite decarburized depth" and the soaking time at 760 °C and 850 °C can be established as Eq. (12)(13) with the same method in Section 3.2, which is shown in Fig. 14. The error bars show the standard deviation, which is caused by repeated measurement. Although the oxidation loss depth has been considered, the "true ferrite decarburized rate" at 850 °C is still lower than that at 760 °C. The reason why the ferrite decarburized depth at 850 °C is smaller than that at 760 °C is not only the oxidation loss, but also the different decarburized mechanism between the two temperature ranges of A_{C1}-A_{C3} and A_{C3}-G.

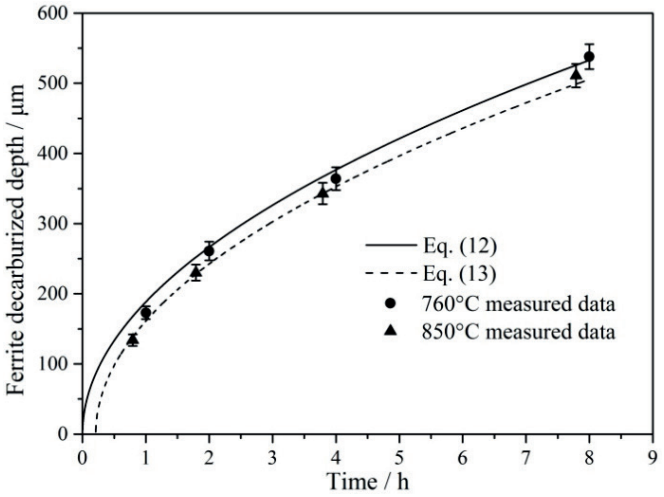

Fig. 14. Relationship between "true ferrite decarburized depth" and soaking time

$$h_4(\mathrm{m}) = 3.14 \times 10^{-6}\sqrt{t(\mathrm{s})} \tag{12}$$

$$h_5(\mathrm{m}) = 3.02 \times 10^{-6}\sqrt{t(\mathrm{s}) - 750} \tag{13}$$

TABLE 4

Oxidation loss depth

Soaking time	12.5 min	1 h	2 h	4 h	8 h
A_{C1}-A_{C3}: 760 °C, oxidation loss depth / μm	--	25	35	56	86
A_{C3}-G: 850 °C, oxidation loss depth / μm	12	40	60	87	120

TABLE 5

The new set of oxidation loss data

Soaking time / s	0	3600	7200	14400	28800
A_{C1}-A_{C3}: 760 °C, oxidation loss depth / μm	0	25	35	56	86
Soaking time / s	0	2850	6450	13650	28050
A_{C3}-G: 850 °C, oxidation loss depth / μm	0	28	48	75	108

TABLE 6

The "true ferrite decarburized depth"

Soaking time / s	0	3600	7200	14400	28800
A_{C1}-A_{C3}: 760 °C, true ferrite decarburized depth / μm	0	173	261	364	538
Soaking time / s	0	2850	6450	13650	28050
A_{C3}-G: 850 °C, true ferrite decarburized depth / μm	0	134	230	343	511

3.4. The relationship between ferrite decarburized depth and decarburized mechanism in different temperature ranges

Above all, the reasons of different decarburized rate in the three temperature ranges are various and complex, but are all in close relationship with the decarburized mechanism.

The ferrite decarburization under A_{C1} temperature is slower than that in the other two temperature ranges. That's because the chemical bond of Fe_3C is more potent on fixing carbon than austenite. In other words, cementite dissolution under A_{C1} temperature is more difficult to proceed than γ→α phase transformation in temperature range of A_{C1}-G.

In temperature range of A_{C1}-A_{C3} and A_{C3}-G, the ferrite decarburization both proceeds through γ→α phase transformation, but the decarburized depth at 760 °C (A_{C1}-A_{C3}) is bigger than that at 850 °C (A_{C3}-G) for a same soaking time. Based on the experimental results, we can know that three reasons lead to this phenomenon. At first, the oxidation loss of ferrite decarburization at 850 °C is bigger than that at 760 °C. This reason is well known and generally accepted. The second, an "incubation period" must pass away before ferrite decarburization occurs at 850 °C. The "incubation period" affects the ferrite decarburized depth signally in short soaking time. The last but not least, the diffusion coefficient of carbon in ferrite is considerably higher than that in austenite, which can be estimated with the Arrhenius equation:

$$D = D_0 \exp(-Q/\mathrm{R}T) \tag{14}$$

where D_0 is the diffusion constant / ($m^2 \cdot s^{-1}$), Q is the activation energy / ($J \cdot mol^{-1}$), R is 8.314J·(mol·K)$^{-1}$, T is the temperature, K. The diffusion constant and activation energy of carbon in ferrite and austenite are D_0^{α}=0.2×10^{-5} $m^2 \cdot s^{-1}$, D_0^{γ}=2.0×10-5 $m^2 \cdot s^{-1}$, Q^{α}=84×10^3 $J \cdot mol^{-1}$, Q^{γ}=140×10^3 $J \cdot mol^{-1}$ [15]. Then the carbon diffusion coefficient in ferrite at 760 °C and in austenite at 850 °C can be estimated as 1.13×10^{-10} $m^2 \cdot s^{-1}$ and 6.16×10^{-12} $m^2 \cdot s^{-1}$, respectively. The former is considerably larger than the latter. The unchanged partial decarburized depth at 850 °C shows that the ferrite decarburized rate is limited to being equal to the partial decarburized rate at A_{C3}-G temperature, which means that the ferrite decarburization is weakened by the carbon diffusion in austenite. In contrast, the ferrite decarburization at 760 °C proceeds through carbon diffusion in ferrite all the time.

4. Conclusions

Through a series of experiments, the decarburized mechanism of high silicon spring steel in three temperature ranges was studied comprehensively. The reason of different ferrite decarburized rate in different temperature ranges was also clear. The following conclusions were obtained:

1. Under A_{C1} temperature, pearlite spheroidization and surface decarburization are carried out simultaneously and pearlite spheroidization is reinforced. Because the chemical bond of Fe_3C is more potent on fixing carbon than austenite, the decarburization under A_{C1} temperature is far slower than that at A_{C1}-A_{C3} and A_{C3}-G temperature.
2. The ferrite decarburized depth follows a parabolic law with the increase of the heating time. Functional relation between the ferrite decarburized depth and the soaking time at 730 °C (< A_{C1}), 760 °C (A_{C1}-A_{C3}) and 850 °C (A_{C3}-G) follows the formula of $h_1(\mathrm{m}) = 1.66 \times 10^{-6}\sqrt{t(\mathrm{s})}$, $h_2(\mathrm{m}) = 2.64 \times 10^{-6}\sqrt{t(\mathrm{s})}$ and $h_3(\mathrm{m}) = 2.38 \times 10^{-6}\sqrt{t(\mathrm{s}) - 750}$, respectively.
3. Considering the oxidation loss depth, the "true ferrite decarburized rate" at 850 °C is still lower than that at 760 °C. This indicates that the reason why the ferrite decarburized depth at 850 °C is smaller than that at 760 °C is not only the oxidation loss, but also the different decarburized mechanism between the two temperature ranges of A_{C1}-A_{C3} and A_{C3}-G.
4. In the temperature range of A_{C3}-G, an "incubation period" must pass away before ferrite decarburization occurs, which affects the ferrite decarburized depth signally in short soaking time. The ferrite decarburized rate is limited to being equal to the partial decarburized rate, which means that the ferrite decarburization is weakened by the carbon diffusion in austenite.

REFERENCES

[1] Y.B. Liu, W. Zhang, Q. Tong, L.F. Wang, ISIJ Int. 54, 1920 (2014).

[2] K. Adamaszek, P. Bro, J. Kucera, Defect Diffus. Forum 194-199, 1701(2001).

[3] M. Nomura, H. Morimoto, M. Toyama, ISIJ Int. 40, 619 (2000).

[4] D.J. Li, D. Anghelina, D. Burzic, J. Zamberger, R. Kienreich, H. Schifferl, W. Krieger, E. Kozeschnik, Steel Res. Int. 80, 298 (2009).

[5] Y. Prawoto, M. Ikeda, S.K. Manville, A. Nishikawa, Eng. Failure Anal. 15, 1155 (2008).

[6] T. Nakano, T. Sakakibara, M. Wakita, Atsushi Sugimoto, JSAE Rev. 22, 337 (2001).

[7] Y. Akiniwa, S. Stanzl-Tschegg, H. Mayer, M. Wakita, K. Tanaka, Int. J. Fatigue 30, 2057 (2008).

[8] M.J. Gildersleeve, Mater. Sci. Technol. 7, 307 (1991).

[9] B. Chehab, H. Zurob, D. Embury, O. Bouaziz, Y. Brechet, Adv. Eng. Mater. 11, 992 (2009).

[10] M. Delince, Y. Brechet, J.D. Embury, M.J.D. Geers, P. Jacques, T. Pardoen, Acta Mater. 55, 2337 (2007).

[11] C.L. Zhang, L.Y. Zhou, Y.Z. Liu, Int. J. Miner., Metall. Mater. 20, 720(2013).

[12] C.L. Zhang, Y.Z. Liu, L.Y. Zhou, C. Jiang, Jin-fu Xiao, Int. J. Miner., Metall. Mater. 19, 116 (2012).

[13] F. Zhao, C.L. Zhang, Q. Xiu, Y. Tan, S.Y. Zhang, Y.Z. Liu, Mater. Sci. Forum 817, 132 (2015).

[14] R.P. Smith, Trans. Metall. Soc. AIME 224, 105 (1962).

[15] G. Parrish, Carburizing: Microstructures and Properties, 1999 ASM International.